Received: 30 August 2017 | Revised: 29 January 2018 | Accepted: 4 February 2018

DOI: 10.1111/bre.12281

ORIGINAL ARTICLE

WILEY Basin Research IAS EAGE

Characterization of the depocenters and the basement structure, below the central Chile Andean Forearc: A 3D geophysical modelling in Santiago Basin area

Felipe Andrés González[1] | Andrei Maksymowicz[1,2] | Daniel Díaz[1,2,3] | Luis Villegas[1] | Maximiliano Leiva[1] | Bárbara Blanco[1,2] | Emilio Vera[1,2] | Sergio Contreras[1] | Daniel Cabrera[1] | Sylvain Bonvalot[4]

[1]Núcleo de Geofísica Aplicada, Departamento de Geofísica, Facultad de Ciencias Físicas y Matemáticas, Universidad de Chile, Santiago, Chile

[2]Departamento de Geofísica, Facultad de Ciencias Físicas y Matemáticas, Universidad de Chile, Santiago, Chile

[3]Centro de Excelencia en Geotermia de Los Andes, Santiago, Chile

[4]Géosciences Environnement Toulouse, Observatoire Midi-Pyrénées, Toulouse, France

Correspondence
Felipe Andrés González, Núcleo de Geofísica Aplicada, Departamento de Geofísica, Facultad de Ciencias Físicas y Matemáticas, Universidad de Chile, Blanco Encalada #2002, Santiago, Chile.
Email: fgonzalezr@ngachile.cl

Present address
Bárbara Blanco, Vicepresidencia de Proyectos, Corporación Nacional del Cobre (CODELCO), Santiago, Chile.

Funding information
Programa de Riesgo Sísmico of the University of Chile (PRS); Núcleo de Geofísica Aplicada (NGA); Departamento de Geofísica of the University of Chile

Abstract

Since the last century, several geological and geophysical studies have been developed in the Santiago Basin to understand its morphology and tectonic evolution. However, some uncertainties regarding sedimentary fill properties and possible density anomalies below the sediments/basement boundary remain. Considering that this is an area densely populated with more than 6 million inhabitants in a highly active seismotectonic environment, the physical properties of the Santiago Basin are important to study the geological and structural evolution of the Andean forearc and to characterize its seismic response and related seismic hazard. Two and three-dimensional gravimetric models were developed, based on a database of 797 compiled and 883 newly acquired gravity stations. To produce a well-constrained basement elevation model, a review of 499 wells and 30 transient electromagnetic soundings were used, which contribute with basement depth or minimum sedimentary thickness information. For the 2-D modelling, a total of 49 gravimetric profiles were processed considering a homogeneous density contrast and independent regional trends. A strong positive gravity anomaly was observed in the centre of the basin, which complicated the modelling process but was carefully addressed with the available constrains. The resulting basement elevation models show complex basement geometry with, at least, eight recognizable depocenters with maximum sedimentary infill of ~ 500 m. The 3-D density models show alignments in the basement that correlates well with important intrusive units of the Cenozoic and Mesozoic. Along with interpreted fault zones westwards and eastwards of the basin, the observations suggest a structural control of Santiago basin geometry, where recent deformation associated with the Andean contractional deformation front and old structures developed during the Cenozoic extension are superimposed to the variability of river erosion/deposition processes.

1 | INTRODUCTION

The Santiago Basin is located in the Chilean margin around 33.5°S, and corresponds to the northern zone of the Central Depression, which is an elongated low topographic morphological feature of the Andean forearc. The Central Depression is bounded to the east by the Andean Cordillera and to the west by the Coastal Cordillera (Figure 1). The Santiago Basin has been partially filled by fluvial sediments, glaciofluvial and volcanic deposits, whose provenance is associated with the Maipo and Mapocho River canyons (Falcón, Castillo, & Valenzuela, 1970). Within the sedimentary infill, isolated hills emerge (Santa Lucía, San Cristóbal, Blanco, Calán, Lo Aguirre, Renca, among others).

Since the 1950s, several geological and geophysical studies have been developed in the Santiago Basin to understand its morphology and tectonic evolution. Between these studies, Kausel (1959) estimated a sediment thickness of approximately 400 m around the city of Santiago based on gravimetric studies and Dragicevic (1982) made gravimetric measures concluding that the basement depth in the Rinconada de Lo Aguirre area (Figure 1) is similar as in the centre of the basin, or that the sedimentary fill density in that area is lower than the rest of the basin. Recent studies present more complete models of the basin geometry by gravity modelling (Araneda, Avendaño, & Merlo, 2000; Yáñez, Muñoz, Flores-Aqueveque, & Bosch, 2015); however, the implications of the underlying bedrock density structure, and the associated uncertainty for the sedimentary fill density/thickness estimations have not been studied in detail. To get a coherent interpretation with the geology and tectonic processes, this study presents new 2-D and

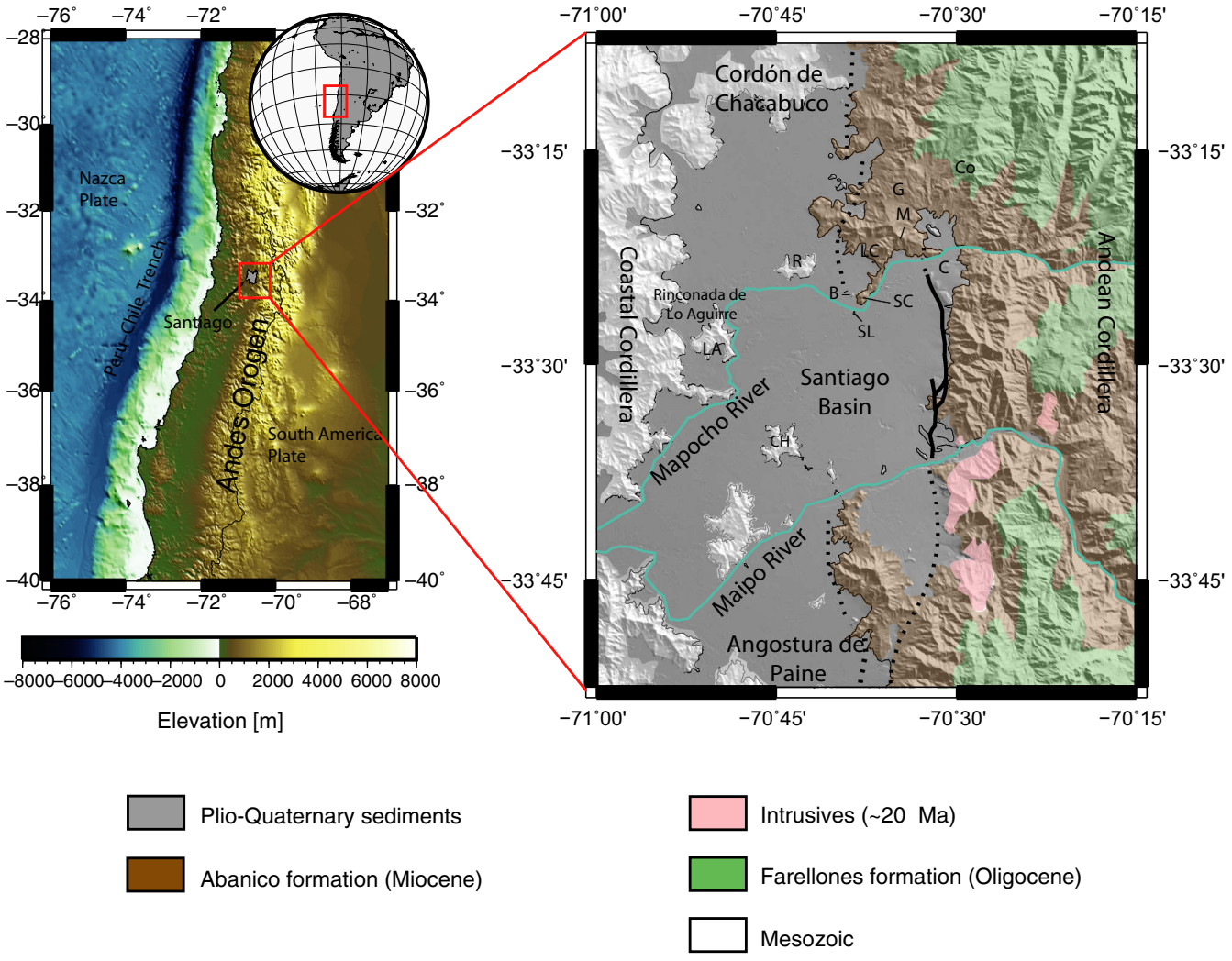

FIGURE 1 Location and geology of the studied area. The left panel shows the regional elevation map around the studied area. The studied area is highlighted in red. The right panel shows a simplified geological map of the studied area and the location of the Andean deformation front. The black line indicates the trace of San Ramon fault observed in the surface, and the dotted line corresponds to the inferred trace of Andean deformation front to the north and to the south. B: Blanco hill, C: Calán hill, CH: Chena hill, Co: Conchalí hill, G: Gordo hill, LA: Lo Aguirre hill, LC: Las Canteras hill, M: Manquehue hill, R: Renca hill, SC: San Cristóbal hill, SL: Santa Lucía hill

3-D gravimetric models of the Santiago Basin constrained with transient electromagnetic data (TEM), integrated with boreholes and wells data. The main objective of this research was to study the morphology and basement inhomogeneities of the Santiago Basin, and their implications for the seismic hazard and the long term Central Andes forearc evolution. For this purpose, 49 2-D profiles were modelled and interpreted and two 3-D gravity models were obtained in the centre of the basin and the entire basin based on high- and low-resolution data respectively.

2 | TECTONIC AND GEOLOGICAL SETTING

The tectonic evolution of the region is characterized by subduction in the western border of South America since at least Mesozoic times (Pardo-Casas & Molnar, 1987). Currently, the oceanic Nazca plate is subducting below the continental South American plate with a convergence rate of 6.6 cm/yr (Angermann, Klotz, & Reigber, 1999). In this context, the Central Depression corresponds to a forearc basin, whose basement is composed by Eocene to Early Miocene volcano-sedimentary rocks (Sellés & Gana, 2001), filled by Pleistocene–Holocene alluvial, fluvial and pyroclastic deposits (Figure 1). In the studied area, the Andes Cordillera front consists mainly of extensional basin-related deposits of the Abanico Formation (late Eocene to early Miocene) overlain by the Miocene volcanic Farellones Formation (Charrier et al., 2002; Thiele, 1980). According to Charrier et al. (2002), the deposition of the volcano-sedimentary units of Abanico formation, in an extensional system, began in the late Eocene, and then, these extensional depocenters were inverted in coincidence with the rapid exhumation of underlying Mesozoic units, and the progressive change in magma composition associated with progressive crustal thickening from mildly tholeitic to calc-alkaline signatures. The tectonic inversion of the Abanico Basin started at the Miocene coetaneously to the emplacement of the Farellones Formation, and even to the younger products of the Abanico Formation, according to Farías et al., 2010).

The scarcity of high-resolution geophysical observations of the upper crustal structure (mainly by the abrupt topography of the Andes and the presence of high populated areas in the forearc) has contributed, in part, to open a debate on the structural style of the compressive deformation currently observed. While numerous authors argue in favour of an eastward migration of the Andean deformation in an east-vergent structural system (Farías et al., 2010; Ramos, Zapata, Cristallini, & Introcaso, 2004; and references therein), Armijo et al. (2010) proposed a west-vergent fold and thrust system with a deformation front coincident with the San Ramón Fault in the eastern border of Santiago (Figure 1). However, at larger scale, the structure of the Andean forearc has been established by traveltime seismic and surface waves tomographies (Farías et al., 2010; Marot et al., 2014; Porter et al., 2012). These models show high body waves velocities, low P-wave to S-wave velocity ratio (Vp/Vs), and low attenuation in the forearc region, contrasting with the opposite tendencies below the Andes Cordillera. Then the geophysical evidence shows a cool and rigid forearc that supports fragile intra-plate deformation, and a shallow fragile-ductile discontinuity below the high elevations of the Andes as showed also by flexural analysis (Maksymowicz, 2007; Tassara, 2005). This rheological behaviour should be considered as an important control for the deformation style present in the margin (Echaurren et al., 2016; Farías et al., 2010).

At local scale, numerous outcrops observed in Santiago basin correspond to volcanic episodes and intrusive rocks (Drake, Curtiss, & Vergara, 1976; Gana & Wall, 1997; Sellés, 1999; Thiele, 1980; Vergara, López-Escobar, Palma, Hickey-Vargas, & Roeschmann, 2004; Vergara, Morata, Villarroel, Nyström, & Aguirre, 1999). These rocks can be associated to magmas with composition from basaltic to rhyolitic–dacitic, and present ages between 11 and 27 Ma. According to Charrier et al. (2002) and Nyström, Vergara, Morata, and Levi (2003), during the late Oligocene, the Chilean subduction margin was characterized by a low convergence rate that favoured the formation of volcanic sedimentary basins. Vergara et al. (2004) suggested that during the early Miocene, new volcanic activity started in the same area as Oligocene volcanism, and at least five large dome complexes or their intrusive equivalents grew in this area, leaving what we recognize today as Las Canteras (22.3 Ma), San Cristobal, Renca (21.8 Ma), Gordo (21.1 Ma) and Santa Lucía (21.2–20.3 Ma) hills (see Figure 1), with a basaltic to andesitic signature, that overlie the deposits of the Oligocene volcanic episodes. A third volcanic episode is recognized during the early Miocene, producing the dacitic porphyries of the Manquehue hill (20.3–19.5 Ma) and some satellite intrusions. Younger volcanic expressions have been found in some places, as the andesitic dyke that outcrops at San Cristobal hill (13.1 Ma) that could belong to some later small-scale volcanic episodes (Vergara et al., 2004). It is important to note that the location of volcanic centres and intrusives suggests a structural control related to the main fault zones involved in the Miocene tectonic extension, as suggested by Fock (2005).

3 | DATA AND PROCESSING

3.1 | Gravity

The gravimetric database includes 1680 gravimetric stations. About 883 of them are new gravity data acquired by

our group in different areas of the Santiago Basin during 2015 (blue dots in Figure 2). The other stations correspond to a compilation of several campaigns (red dots in Figure 2): 233 gravity stations acquired during the Anillo Project (ACT N°18) of the University of Chile between 2007 and 2010, 183 stations acquired by the Centro de Excelencia en Geotermia de Los Andes (CEGA) during 2012, 227 stations registered in 1959 by Edgar Kausel (Kausel, 1959), and 154 gravity points from numerous short campaigns performed by the Departmento de Geofísica of the University of Chile (DGF).

The acquisition of new data was funded by the *Programa de Riesgo Sísmico* of the University of Chile (PRS), using a CG-3 Scintrex gravimeter provided by the IRD-GET (Géosciences Environnement Toulouse). The gravimetric campaign was conducted between 7 January and 21 August 2015, where 19 profiles and 2 meshes of gravity stations were acquired. The spacing between stations was 500 m and 1000 m for profiles and meshes respectively (see Figure 2). The elevation data were acquired using a Topcon HiperV dGPS system and the considered gravimetric base corresponds to the absolute gravity point located in the Hall of the DGF building (979416.042 mGal, 2012).

Due to the variable sources of gravity stations, it was necessary to check and validate the gravimetric and topographic references of different campaigns to build a coherently merged database. For this purpose, a levelling process was conducted to bring all the gravity data to the same reference value (absolute gravity measurement at DGF). In addition, new gravimetric and dGPS measurements were registered in the same positions of several stations originally acquired by Kausel and Anillo project, in order to verify elevations and to translate these databases to the new gravimetric and topographic references.

The accepted standard deviation for gravity measurements was approximately 0.1 mGal, with a minimum of 0.01 mGal and a maximum of 0.6 mGal. The larger deviations were accepted in measurements carried out in difficult logistic conditions. Any point with larger error was repeated immediately in field. On the other hand, the adjusting error for the post-processing dGPS data elevation was approximately +−0.1 m, which imply a maximum error of +−0.03 mGal in the free air correction and +−0.01 in the Bouguer correction. Then, the total standard deviation for the computed complete Bouguer anomaly was +−0.12 mGal.

The gravity data were processed to obtain the complete Bouguer anomaly (Figure 2) by applying standard corrections: Instrumental drift correction by removing a time-linear trend between the gravity values registered in daily repetitions of the base station; Tide correction applying the Longman (1959) algorithm; Normal gravity correction by subtracting the theoretical gravity of the WGS-84 ellipsoid, free air and Bouguer corrections based on the D-GPS ellipsoidal altitude and a reference density of 2.67 g/cc; and finally, a Terrain correction by using a GDEM elevation grid of 30 m × 30 m resolution. Free air, Bouguer and Terrain corrections were computed in Geosoft-OasisMontaj software, and the final grids for interpretations were generated with the minimum curvature interpolation method in the Generic Mapping Tools software package (GMT).

Afterwards, 49 gravity profiles distributed throughout the Santiago Basin were modelled using the ENCOM-ModelVision software, to obtain a gravimetric 2-D model.

3.2 | Gravity model constraints

To constrain at least a minimum sedimentary thickness, 30 TEM data stations (cyan filled boxes in Figure 2) and 499 boreholes data (Falcón et al., 1970; Karzulovic, 1957; see black filled circles in Figure 2) were used (see Figure 2 and supplementary material).

TEM stations were distributed in the study area according to the spatial availability of free empty areas. The acquisition was carried out with a WalkTEM equipment using a central loop configuration, with power transmission in 40 m × 40 m or 100 m × 100 m square loops. The resistivity-depth models were obtained by inversion of the observed data employing the IX1D-INTERPEX software using a least squares algorithm.

3.3 | 3D gravity modelling

The 2-D gravity modelling process is aimed at obtaining a sedimentary infill thickness considering a constant density and a 2-D geometrical approximation, i.e. the basement geometry, topography and gravity slowly varies in a direction perpendicular to the profile. To study the inhomogeneities of the basin, a 3-D model of the study area was obtained using the UBC-GIF GRAV3D v3.0 program library (Li & Oldenburg, 1998) for carrying out a forward modelling and inversion of the gravity data in a 3D volume. This software discretizes the modelled volume in rectangular blocks of constant and independent density contrast values. The inversion aims at recovering a model that reproduces the observed residual gravity data within an error tolerance by minimizing a model norm that measures the roughness of the model, to prevent the occurrence of artefacts. A regularization parameter, μ_0, is chosen for the misfit/norm trade-off. It is selected at the beginning of each iteration, as it gives rise to the expected misfit. This also generates the slope of the misfit curve at μ_0. Using the generated slope, a parameter $\mu=\mu_0$ is then selected and used for the inversion. Further detail of the regularization parameter selection flow chart may be found in GRAV3D v3.0 manual (https://www.eoas.ubc.ca/ubcgif/iag/sftwrdocs/grav3d/grav3d-manual.pdf).

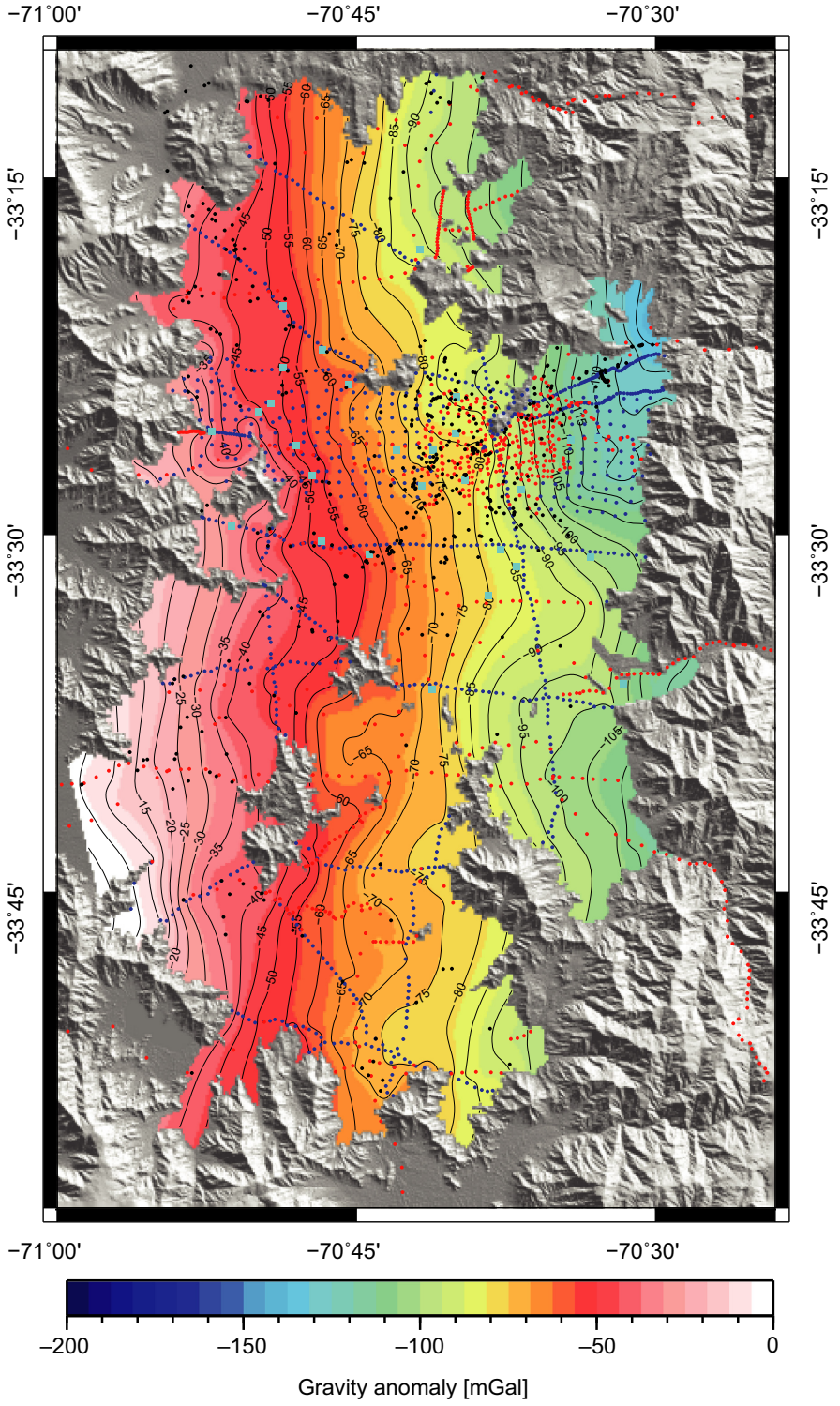

FIGURE 2 Complete Bouguer anomaly in the Santiago basin. The gravity stations location from the PRS project and other compiled campaigns are plotted as blue filled circles and red filled circles respectively. The TEM stations and integrated wells and boreholes are plotted as cyan filled boxes and black filled circles respectively

4 | RESULTS

4.1 | Gravity anomaly

Figure 3a shows the gravity anomaly resulting from the subtraction of the regional trend from the complete Bouguer anomaly (CBA) (Figure 2). The main regional trend corresponds to an almost constant eastward gravity gradient in response to the presence of the continental root below the Andes, at depths larger than 40 km. This removal of the regional signal was carried out extracting the best plane passing through the CBA points. The resulting residual Bouguer anomaly (RBA) brings the first clues about the morphology of the Santiago Basin.

The existence of a prominent positive anomaly of long wavelength becomes evident towards the centre of the

basin (Figure 3a), with values between 5 and 20 mGal. The presence of this anomaly makes it impossible to consider only one linear regional trend to model the sedimentary thickness in the long east–west 2-D lines, because the biggest part of the signal is probably generated by positive density anomalies below the top of the basement, which introduce a trade-off between basin geometry and basement inhomogeneities.

To make a preliminary and qualitative interpretation of the Santiago Basin, the Figure 3b shows the residual filtered Bouguer anomaly obtained after the application of a high-pass filter with a cut-off wavelength of 20 km over the RBA anomaly. In this figure, it is possible to recognize at least eight depocenters distributed throughout the basin. These depocenters show negative gravity anomalies between −4 and −13 mGal, and are limited by lineaments of high gravity in a NE–SW direction as seen in the area between San Cristobal and Cerro Chena hills.

4.2 | 2-D density models

To characterize the basin morphology, the sedimentary infill was modelled with a homogeneous density. Previous studies have adopted a wide range of density values. Particularly, Bonnefoy-Claudet et al. (2009) presented a density range between 1.15 g/cc and 2.3 g/cc. Yáñez et al. (2015) used a range of densities between 1.72 g/cc and 2.08 g/cc based on sediments classification and empirical density conversions. An interesting observation comes from Pilz et al. (2010), who observed shear wave velocities

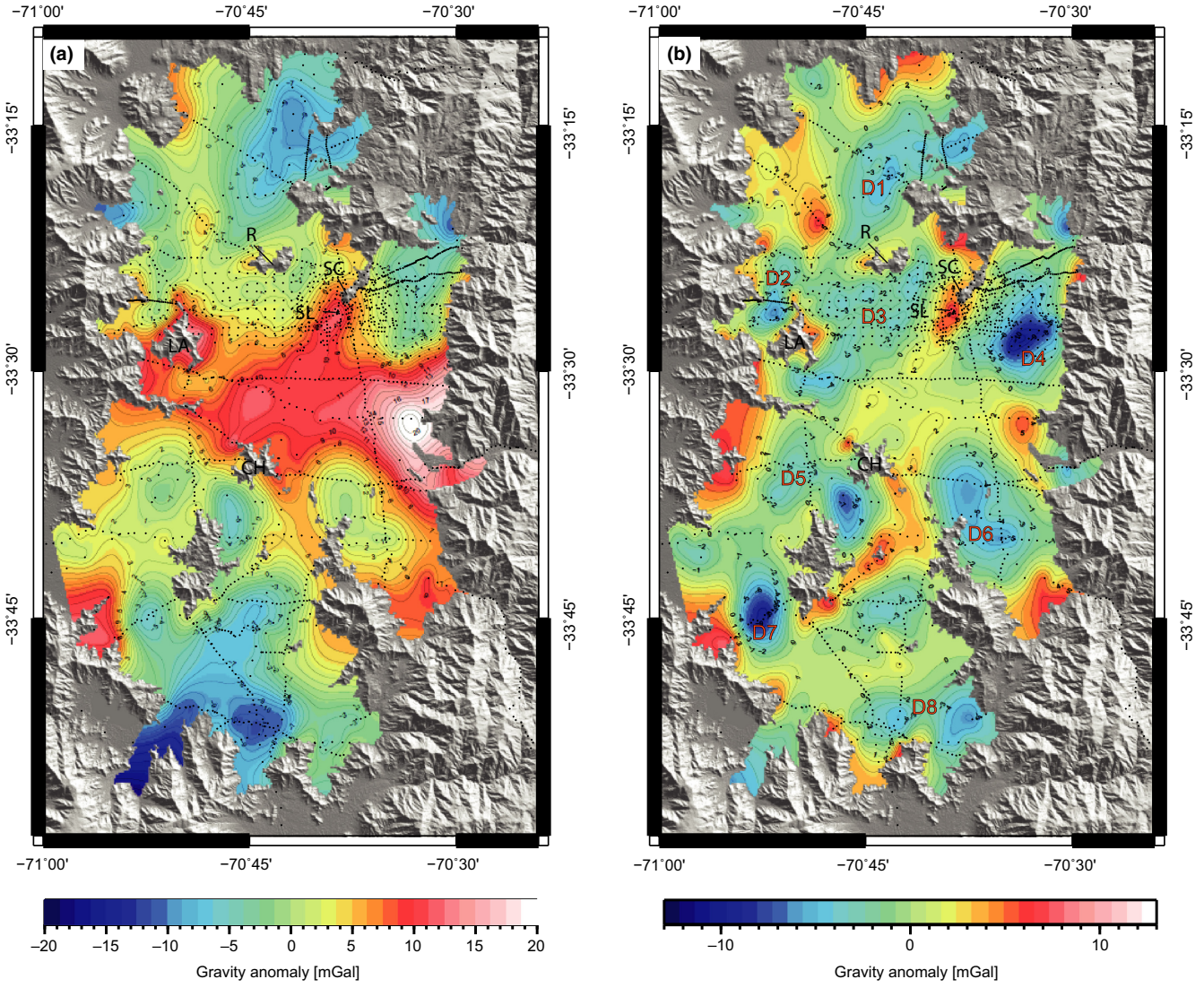

FIGURE 3 Residual gravity anomaly in the Santiago basin. (a) The result from the regional trend extraction of the CBA (Figure 2), while (b) shows the RBA spatially filtered based on the application of a high-pass filter with a cut-off wavelength of 20 km. The location of eight identified depocenters is shown in (b) (D1-D8) and the gravity stations are plotted as black filled circles.CH: Chena hill, LA: Lo Aguirre hill, R: Renca hill, SC: San Cristóbal hill, SL: Santa Lucía hill

>1000 m/s in the sedimentary infill of the basin, suggesting density values slightly higher than 2 g/cc (Seno, 2009). In the present work, it has been considered that while the density values at the surface may be smaller than 2 g/cc, it should increase in depth by compaction processes. Additionally, the independent constraint of TEM models and wells shows that a density contrast of 0.57 g/cc (2.67 g/cc bedrock density) is necessary to obtain realistic sedimentary thicknesses. Thus, a value of 2.1 g/cc was chosen to model the sedimentary fill.

Figure 4 shows two examples of the 49 2-D profiles modelled in the Santiago Basin (all profiles can be observed in the supplementary material). The location of the modelled profiles can be observed in Figure 5. As observed in Figure 4, an independent linear regional trend was considered for each profile according to the existence of bedrock outcrops at the ends. Due to the complexity of the gravimetric signal (see Figure 3) and the probable existence of high-density anomalies below the basin (see section 4.1), this "hill to hill" regional trend definition allowed to estimate the sedimentary thickness along individual profiles, keeping the large wavelength anomalies represented by variations of the gravity regional in the different profiles. However, in the case of 2-D profiles located in the central portion of Santiago basin, the distance between basement outcrops is large and linear regional trend makes no sense. In those cases, it was necessary to split the regional trend in linear segments using available independent constraints of sedimentary thickness near the centre of the basin (Figure 4a). Unfortunately, available constraints of basement depths are scarce, and the TEM models and wells information allow, in general, estimations of minimum sedimentary thicknesses (see discussion in section 5). An example of this uncertainty is observed in the profile PC44 (Figure 4a), which is in the central-south area of the basin between the Rinconada de Maipú sector and the Andean Cordillera. This profile is constrained by sediment thickness data from a well (HU1) and six TEM stations. Two different linear regional trends were used in the same section to account for the bedrock exposure at the ends of the profile and the different regional behaviour between the eastern and western parts.

On the other hand, a simple gravity trend is enough to model short profiles, as observed for the PC32 profile (Figure 4b), which is located in the central-south area of the basin, between the Chena hill and the Cordillera de Los Andes. This profile is characterized by a negative residual anomaly, which results in a maximum sediment thickness of about 500 m in the depocenter D6.

The results of the 2-D modelling process are shown in Figure 5. In this figure, values of basement elevation (Figure 5a) and sediment thickness (Figure 5b) were derived from the 2-D sections interpolation. Analysing the basement elevations, it is possible to recognize the same depocenters previously observed in Figure 3b as negative gravity anomalies.

In the northern sector of the basin, where there is a low density of data measurements, a depocenter (D1) is observed with a maximum sedimentary thickness of about 320 m, which is limited by Cordón de Chacabuco to the north, Renca and Lo Aguirre hills to the south-east and south-west respectively, the Coastal Cordillera to the west and Chicureo to the east. This depocenter is connected to two other depocenters located southwards (D2 and D3). Aligned at similar latitude, D2, D3 and D4 define a sector with maximum thicknesses higher than 400 m (>500 m in D4), locally interrupted by the San Cristobal and Lo Aguirre hills (see Figure 5a). This area is sampled by a good distribution of gravimetric stations and additional information from boreholes and TEM data.

To the south, the central area of the basin is sampled by a lower amount of gravimetric stations, and the presence of the large positive gravity anomaly in the centre of the basin makes difficult the modelling and interpretation processes (Figure 3). However, we observed a decrease of sedimentary thickness in the centre of the basin (Figures 4a and 5b), which is similar to that obtained in the well-constrained models to the north, suggesting a north–south continuity of the depocenters in this zone of the basin. Southward, the location of Cerro Chena hill in the middle of the basin, and small hills around it, allows to reduce the uncertainties of the gravity regional trend. Here the 2-D modelling shows two prominent depocenters (D5 and D6). D5 shows a maximum thickness of about 350 m, and D6, located in Puente Alto area (immediately to the west of the large Maipo River canyon), reaches 500 m of maximum sedimentary thickness (Figure 4b). It is interesting to note the abrupt eastward increase of the basement elevation observed at the distance x=~11000 m along the PC32 profile (Figure 4b). This basement anomaly correlates well with the presence of the small north–south elongated Cerro Las Cabras hill.

The southern part of the Santiago Basin is located in Talagante and Paine areas, limited to the south by the Angostura de Paine hills. This area is characterized by the presence of two depocenters (D7 and D8). D7 shows a maximum thickness of about 500 m, and the depocenter D8 shows thicknesses between 200 and 500 m.

In general, 2-D modelling allows the geometrical characterization of the depocenters observed as low gravity anomalies in the high-pass filtered version of the Bouguer anomaly (Figure 3b). This means that the "hill to hill" gravity regional trend definition separates the longer wavelength signal from the effects of the sedimentary cover (see more details in supplementary material). However, the 2-D model does not provide information about the meaning of

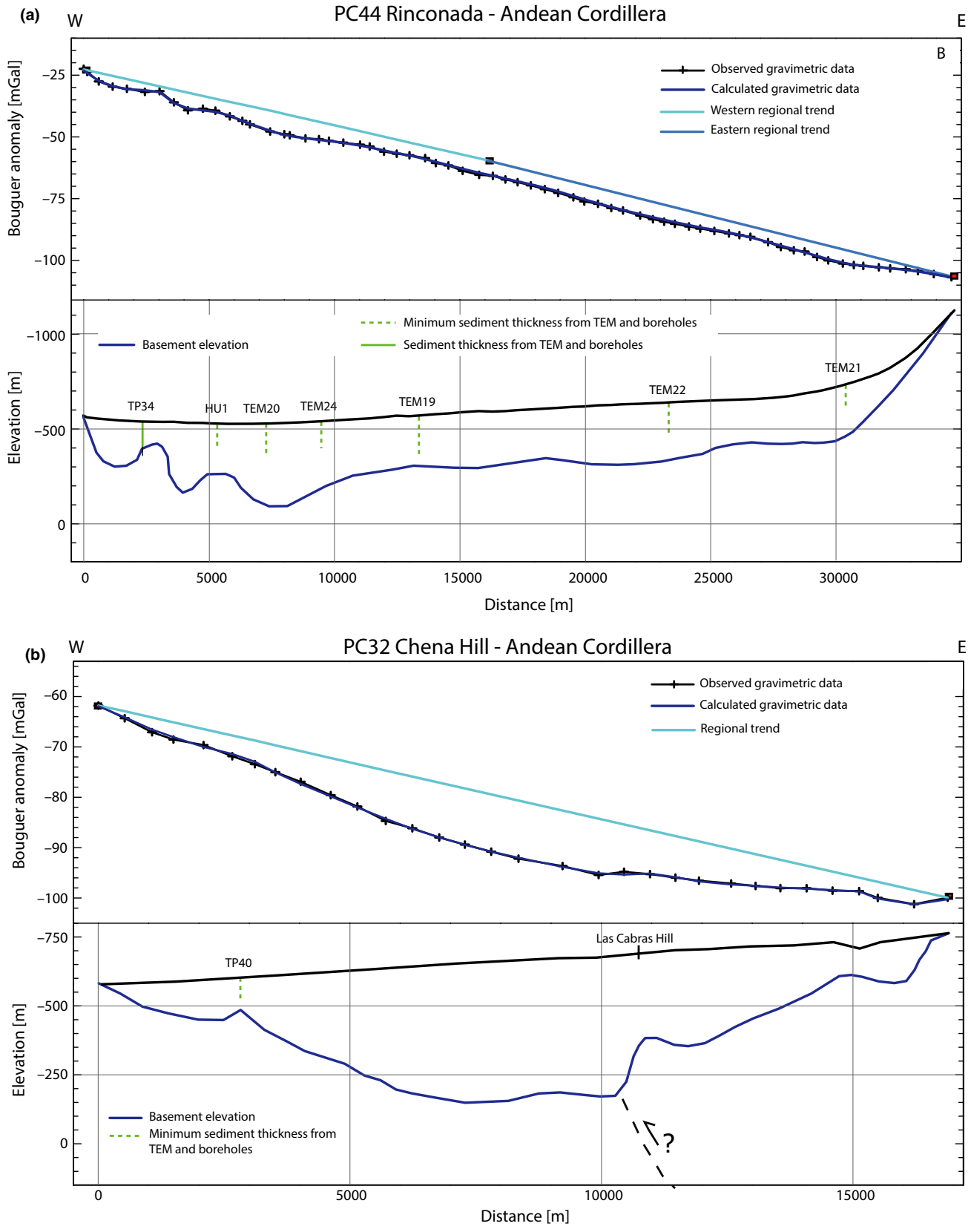

FIGURE 4 2D modelled gravity profiles for PC44 (a) and PC32 (b). The panel above in each figure shows the observed gravity data (black crosses) and theoretical response (blue solid lines). The panel below in each figure shows the elevation section as a result of the inversion process. The black line corresponds to the topographic elevation, while the blue solid lines represent the basement elevation using a bedrock density of 2.67 g/cc

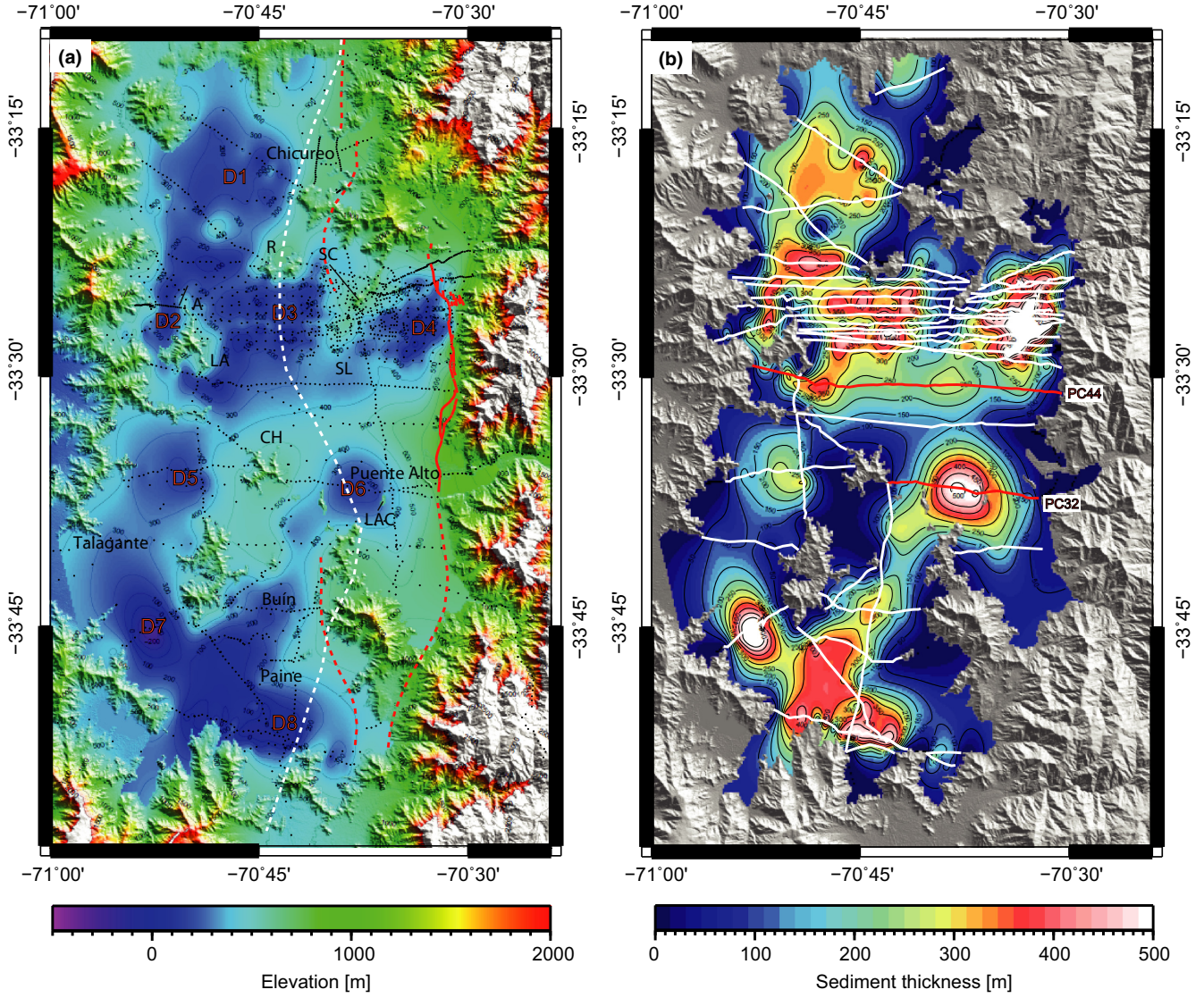

FIGURE 5 Basement elevation (a) and sediment thickness (b) obtained from the 2D gravity models. The gravity stations are shown as black filled circles in the left figure. The modelled 2-D gravity sections are plotted as red and white solid lines in the right figure. The red line in the left figure indicates the trace of San Ramon fault observed in the surface, and the dotted red line corresponds to the inferred trace of Andean deformation front to the north and to the south. The white dotted line in the left figure shows the approximated limit between Cretaceous and Cenozoic units in the basement according to Thiele (1980). A: Amapola hill, CH: Chena hill, LA: Lo Aguirre hill, LAC: Las Cabras Hill, R: Renca hill, SC: San Cristóbal hill, SL: Santa Lucía hill

the large positive Bouguer anomalies, or about the quality of the 2-D assumptions, and for this reason, we performed 3-D inversions of the gravity anomaly to improve the visualization of the Santiago Basin structure.

4.3 | 3-D model of the dense gravity mesh

The large amount of gravity data distributed in the north-central area of the basin (Figure 2) allowed the inversion of a 3D basin model (Figures 6 and 7). The size of the modelled volume is 40 km × 10.5 km × 3.5 km in the E–W, N–S and vertical directions respectively. The volume was discretized in blocks of 100 m × 100 m horizontally, and 25 m vertically. To dissipate border effects, this volume was horizontally extended to a total of 51 km × 21.5 km. The initial model for the inversion is actually an interpolated version of the 2-D model of the basin (section 4.2), which allows some flexibility in density values for the discrete blocks near the contacts interpreted from the 2-D model. This partially constraints the whole 3-D model, as individual blocks have to take their density values from a given range. Then, the resulting 3D models correspond to a 3D density distribution that fit the data and have small differences with the initial 2D models. From the surface to the sediments/basement transition, the densities can vary between the values 1.7 g/cc and 2.1 g/cc. In

the sediments/basement transition zone, centred in the 2-D basement depth model, densities can take values between 1.7 g/cc and 2.67 g/cc. Below the sediments/basement transition zone, the densities ranged from 2.67 g/cc to 2.92 g/cc. The modelled gravity anomaly (see supplementary material) was generated removing a plane trend defined by linear regression of the gravity data located in the borders of the modelled zone. Then, the obtained density structure is representative for the local structure of the north-central area in Santiago basin (Figure 7).

Figure 6 shows the basin geometry derived from the 3-D inversion. The basement depth was defined as the level where the density 2.67 g/cc is observed. As we can see, the general shape and sedimentary thickness have the same characteristics previously observed in the 2-D model (Figure 5). The depocenter D2 geometry is elongated in the north–south directions with a maximum sedimentary thickness below 400 m. To the east, the depocenter D3 shows, in general, sedimentary thicknesses around 400 m and basement elevations near 100 m. In this area, the maximum sedimentary thickness is obtained in a small patch located near the centre of the model with values higher than 450 m. Eastward, the presence of the depocenter D4 characterizes the zone between the San Cristobal Ridge and the Andean deformation front. Here, the basin has an elongated shape with maximum sedimentary thicknesses higher than 650 m. It is interesting to note that D4 presents basement elevations lower than the zero level (Figure 6a), which in comparison to the depocenter D2 and D3, suggests a general eastward deepening of the basement in this region of the Santiago Basin. Another particularity of D4 is the rapid increase of basement elevation (and sedimentary thickness decrease) in the eastern limit of the Santiago Basin, evidenced by the short distance between iso-contours in Figure 6a,b.

Figure 7 shows the obtained density structure at different depths. Under zero level we can see a variable density structure elongated in the east–west direction showing a decrease of heterogeneity with depth. At 200 m of elevation we can see the first evidence of sedimentary infill corresponding to the depocenters observed in Figure 7 (D2, D3 and D4). It is interesting to note that it is possible to see a basement heterogeneity that correlates well with the location of Santa Lucía Hill at surface. This feature is also observed in deeper levels.

4.4 | Large-scale 3-D model

A regional scale 3-D gravity model was performed to make up for the large positive gravity anomaly observed in the centre of the Santiago Basin (see Figure 3a). This model uses the 2-D model of the basin geometry as an initial model to focus the inversion on the density structure of the bedrock.

In this case, the dimension of the selected volume was 55 km × 95 km × 9.5 km in the E–W, N–S and vertical directions, respectively, covering the whole basin and surrounding hills, from an elevation of 4500 masl to a depth of 5000 mbsl. The volume was discretized in blocks of 500 m × 500 m horizontally and 100 m vertically. To dissipate border effects, this volume was horizontally extended to a total of 79 km × 119 km. Infill thickness and density where fixed to match that of the 2-D modelling, with exception of the blocks in the infill-basement boundary, which densities where linearly averaged according to how much infill or basement they encompassed. The basement density range used was 2.57–2.92 g/cc. The modelled gravity anomaly was obtained from the inversion of the residual gravity anomaly data observed on the entire basin (see supplementary material).

The results of the large-scale 3-D modelling are shown in Figure 8, where the basement structure is observed at different depths. The observed heterogeneities are roughly coincident with the Cretaceous and Miocene intrusives at the most important rock outcrops observed in the Santiago Basin. A northwest elongated high-density feature extended between Pirque area and Lo Aguirre hill (LA) explains a large portion of the strong positive gravity anomaly observed at the centre of the basin (Figure 3a).

5 | INTERPRETATION AND DISCUSSION

The obtained 2-D and 3-D models of the Santiago Basin allowed us to describe the basin in terms of its morphology and implications for the tectonic evolution of the area. The features observed in these models could be associated to the paleo-relief of the basement, and also to the tectonic activity of the western border of the Andes Cordillera.

The results obtained at the centre of the basin present uncertainties related to the strong positive anomaly observed in the data (Figure 3a). This anomaly generates a trade-off between the basin geometry and the basement inhomogeneities, which can be solved only by the introduction of independent constrains. However, the available wells in area do not reach the basement and the TEM models in general do not penetrate to the basement depth due to the urban electromagnetic noise (see supplementary material). The discussed trade-off explains the differences in sedimentary thickness in several parts of the basin, observed while comparing the results presented here with those of other models previously published for this area, which present solutions for the basin geometry of an

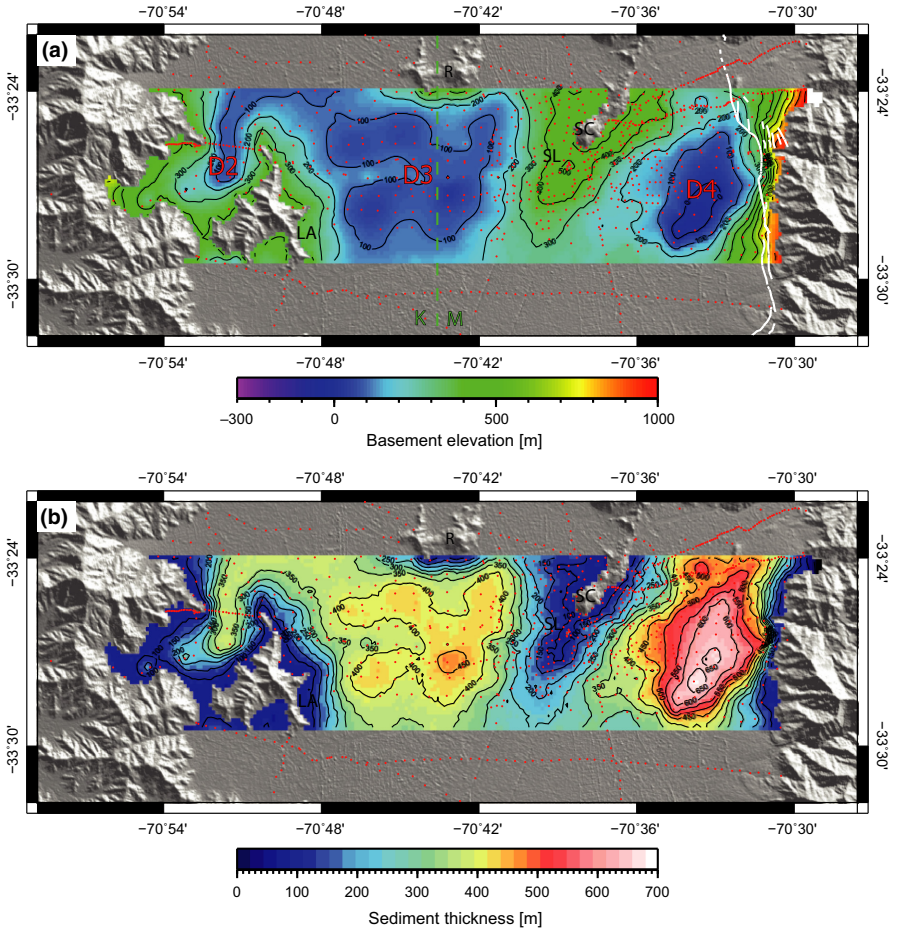

FIGURE 6 Basement elevation (a) and sediment thickness (b) obtained from the 3-D gravity modelling. The gravity stations are shown as red filled circles. The white line in (a) indicates the trace of San Ramon fault observed in the surface. The green dotted line shows the approximated limit between Cretaceous and Cenozoic units in the basement according to Thiele (1980). LA: Lo Aguirre hill, R: Renca hill, SC: San Cristóbal hill, SL: Santa Lucía hill

unconstrained definition of gravity regional trends (Araneda et al., 2000), or assume unconstrained models for basement density variations (Yáñez et al., 2015). Then, the exact values of the basement depth in the centre of the Santiago Basin are not completely solved yet, but, according to new available constraints, the geometry presented here can be considered as a lower boundary for the basement depth. The results enhance the importance of developing new geophysical methodologies that allow the direct observation of the sediments–basement interface below the highly populated zones of the area.

From the large-scale basement elevation (basement relief) model (Figure 5a), we observe that Santiago basin morphology is quite complex, and is characterized by the presence of, at least, eight depocenters with a maximum sediment thickness of around 500 m (Figure 5b). It is interesting to note that, except for D1, all the depocenters are located around the two most important rivers in the region (Mapocho and Maipo Rivers, see Figure 1), which confirms that these rivers play an important role in the erosion and sedimentation of the Santiago Basin (Falcón et al., 1970). In this sense, the results are compatible with the model presented by Farías et al. (2008), where the Central Depression is explained by the erosive influence of the rivers, in response to a general uplift of the forearc (including Coastal Cordillera and Principal Cordillera) after 10 Ma. This interpretation is reinforced by the shape of large depocenters D1, D3 and D8, which present relatively plane (and horizontal) regions at the base, suggesting the presence of peneplains, like the observed by those authors around the basin. However, it is important to note that the minimum basement elevation is approximately 0 m in D3 and D4, while the minimum basement elevation is near −100 m at D8 and lower that −200 m at D7, which imply that a model for the Central Depression formation needs to consider subsidence, at least for the southern portion of the Santiago Basin.

Numerous studies showed the presence of a thrust fault in the eastern limit of the basin (Armijo et al., 2010; Farías et al., 2010; Díaz et al., 2014; Giambiagi et al., 2014; among others). A similar consideration can be made at the PC32 profile, where an important scarp is observed at the eastern edge of the depocenter D6. This feature correlates well with the location of Las Cabras hill and is interpreted as a deep expression of the frontal branch of the San Ramón fault system (Figure 4b). This result corresponds to the first direct observation of the western Andean deformation front in the south-central zone of the Santiago Basin.

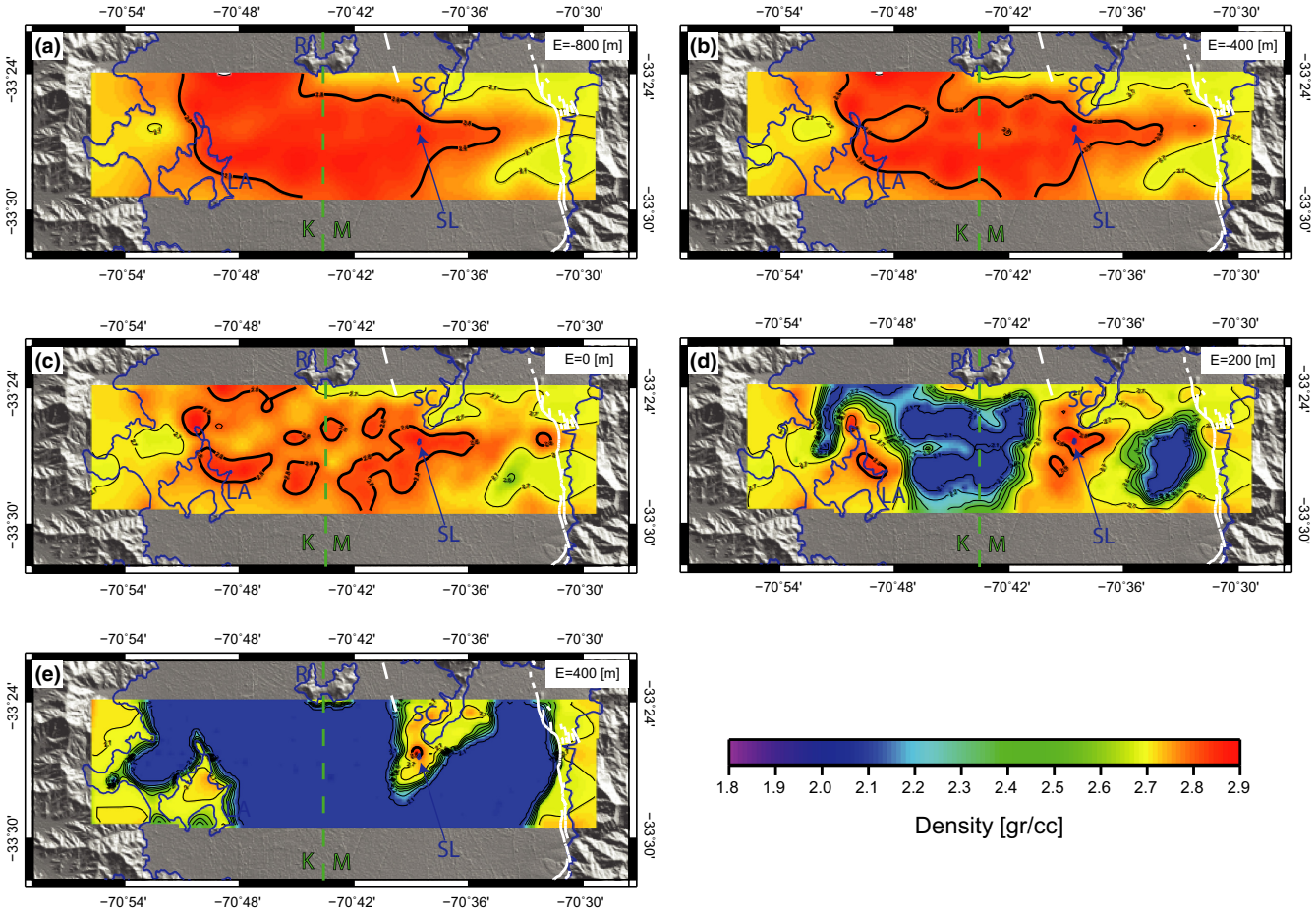

FIGURE 7 Density sections from high-resolution 3D modelling. Each density section corresponds to a elevation value, ranging from −800 to 400 masl (from (a) to (e), respectively). The outline of isolated hills and borders of the basin are shown as blue lines. The white line indicates the trace of San Ramon fault observed in the surface and the dotted white line corresponds to the inferred trace of Andean deformation front to the north and to the south. The green dotted line shows the approximated limit between Cretaceous and Cenozoic units in the basement according to Thiele (1980). LA: Lo Aguirre hill, R: Renca hill, SC: San Cristóbal hill, SL: Santa Lucía hill

The compressive deformation of this structure, and the increase of topographic loading during the Andean uplift, should generate a tilting effect on the forearc, forming a foreland basin (Armijo et al., 2010). However, in general, a systematic eastward decrease of the basin relief is not observed in the model (except for the depocenters D2, D3 and D4, Figure 5a). According to this, the regional signal of the flexure generated by the topographic loading is masked by the erosive processes, but could explain the elevations below the sea level observed in the basement relief.

At local scale, the 3-D inversion of dense gravity mesh allows to obtain detailed models of the elevation and sedimentary thickness in the zone of the depocenters D2, D3 and D4 (Figures 3b and 6). Each one of these depocenters is bounded by low sediment areas that coincide with important features observed at surface (from east to west: Western Cordillera, San Cristobal and Santa Lucia hills, Lo Aguirre, and Coastal Cordillera). We note that the basement elevation slightly decreases to the East (Figure 6a), which could be in part related to the flexural response of Andean topographic load over the continental crust. A particularity of the D4 depocenter is the rapid increase of the basement elevation at the eastern limit of the basin (Figure 6a), which seems to agree with the

FIGURE 8 Density sections from the large-scale 3-D modelling. Each density section corresponds to a elevation value, ranging from −4050 to −450 masl (from (a) to (d), respectively). The outline of isolated hills and borders of the basin are shown as blue lines. The red line indicates the trace of San Ramon fault observed in the surface and the dotted red line corresponds to the inferred trace of Andean deformation front to the north and to the south. The white dotted line shows the approximated limit between Cretaceous and Cenozoic units in the basement according to Thiele (1980). EM: Early Miocene intrusives, EEM: Eocene–early Miocene intrusives, EK: Cretaceous intrusives. CH: Chena hill, LA: Lo Aguirre hill, R: Renca hill, SC: San Cristóbal hill, SL: Santa Lucía hill

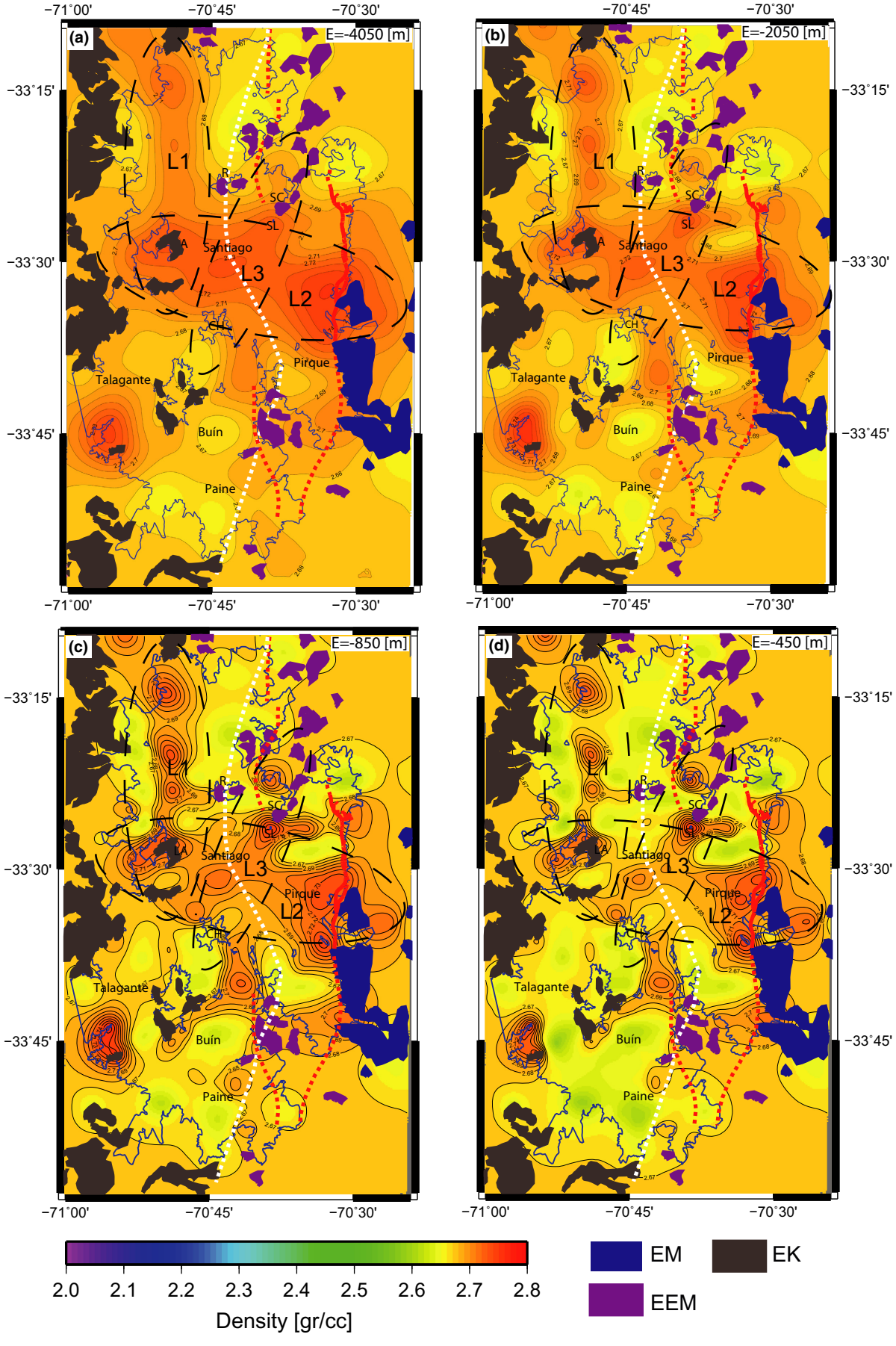
(a)
E=-4050 [m]
(b)
E=-2050 [m]
(c)
E=-850 [m]
(d)
E=-450 [m]
−71°00'
−70°45'
−70°30'
−33°15'
−33°30'
−33°45'
L1
L2
L3
R
SC
SL
LA
CH
Santiago
Pirque
Talagante
Buín
Paine
2.0
2.1
2.2
2.3
2.4
2.5
2.6
2.7
2.8
Density [gr/cc]
EM
EK
EEM

location of the observed San Ramón fault trace at surface, near the western Andean front. South of Renca hill (~70° 43'S) we interpret a slight discontinuity of the basement elevation in the north–south direction (Figure 6). This is observed as a north–south lineament in the basement geometry that could be related to the western limit of the Abanico Formation, which supports the presence of a fault zone for the Mesozoic/Cenozoic boundary (see Figure 1), as was recognized at Renca hill (Thiele, Bobenrieth, & Boric, 1980; Fock, 2005; Gana & Wall, 1997; Fuentes, 2004). All these observations in the detailed 3D model suggest a structural control of Santiago basin geometry, where recent deformation associated to the Andes deformation front and old structures developed during the Cenozoic extension are superimposed to the variability of river erosion/deposition processes.

The density distribution observed in Figure 8 is the result of the large-scale 3-D gravimetric inversion performed to study the basement inhomogeneity. Despite the trade-off between density and depth-extension of the bodies, this model allows the characterization of the main features observed below the basin, their shape and relative magnitude. A north–south high-density lineament is observed in the north-west sector of the basin, linking the Cordón de Chacabuco with the Lo Aguirre area (L1 in Figure 8). Eastward, a second important lineament (L3, Figure 8) extends to the south-west, following the San Cristobal-Santa Lucía belt, and intersecting the previously described elongated east–west feature (L2 in Figure 8). These high-density lineaments correlate with the distribution of Cenozoic and Mesozoic intrusives identified around the basin (Thiele, 1980). In particular, Cretaceous intrusives (EK in Figure 8) seem to be related to L1, whereas Eocene–Miocene (EM-EEM) are associated to L2 and L3. In fact, several density peaks of these linements correlate with Cenozoic volcanic centres and/or intrusives corresponding to basement outcrops observed as isolated hills (Amapola-Lo Aguirre, San Cristóbal and Santa Lucía, etc.), and the Andean and Coastal Cordilleras. Accordingly, the high-density lineaments are close related to the main structures that controlled the evolution of the Andean forearc, revealing the magmatic expression associated to these structures, which were active during the deposition of Abanico and Farellones formations (Farías et al., 2010; Fock, 2005).

The highly populated Santiago Basin is permanently in seismic risk due to the tectonic context of the convergent margin, the complexity of its morphology, and the extensive depocenters located below important populated areas (which are particularly prone to seismic site amplification and its consequential damage over the city.) Pilz et al. (2010) studied the S-wave velocity structure of the Santiago Basin, finding a relationship between the near-surface velocity structure and the observed intensities of the 1985 Valparaiso earthquake and concluding that a more realistic basin model must be developed for the calculation of seismic hazard.

The observed intensities of the 1985 Valparaiso and 2010 Maule earthquakes (Figure 9) (Astroza, Ruiz, Astroza, & Molina, 2012; Menéndez, 1991; Molina, 2011) show significant damage in the north-western part of the city (intensities up to 8.5) and minor to moderate damage in the north-eastern portion (Las Condes and Vitacura area). As observed in H/V and shear wave velocity studies (Leyton et al., 2011; Pastén et al., 2016; Pilz et al., 2010), there is a direct relation between the near-surface mechanical properties and geology (deposits ash interbeds at the West related to low vs. 30 values and sandy gravels of medium to high density at the East related to medium-high vs. 30 values) and the observed intensities in this region. The sediment thickness model presented here shows a correlation between the most damaged zone at the west and the depocenter D3 with a sedimentary thickness of approximately 400 m (Figure 9). However, a depocenter (D4) is also observed below the western part with even a thicker sediment infill (around 600 m) within the area of minor observed damage. Then, the sediment thickness model shows little correlation with the observed seismic intensities in this region, leading to the conclusion that, at least in the northern part of the basin, the near-surface properties may play a more key role on the seismic amplification than the deep structure of the basin.

Other medium to high intensity areas correlate with observed depocenters D5, D7 and D8 in the south-central zone of the basin, where the model shows maximum thicknesses of around 500 m (Figure 9). Although the observed damages in this area have been explained before in terms of the near-surface geology, the direct correlation is not completely supported due to the lack of observed damages and near-surface properties data. In future works it is necessary to study these depocenters in detail and take the basin geometry into account to obtain reliable seismic risk estimations.

6 | CONCLUSIONS

Basement elevation and sedimentary thickness are the most important results obtained by the geophysical model in the Santiago Basin. These products were the main results expected from the analysis of this geophysical data, and their characterization and understanding may play a key role in the estimation of seismic risk in the basin. The morphology of the basement is clearly heterogeneous, as shown by the various geophysical data analysed in this work. It consists of different units with their own relief,

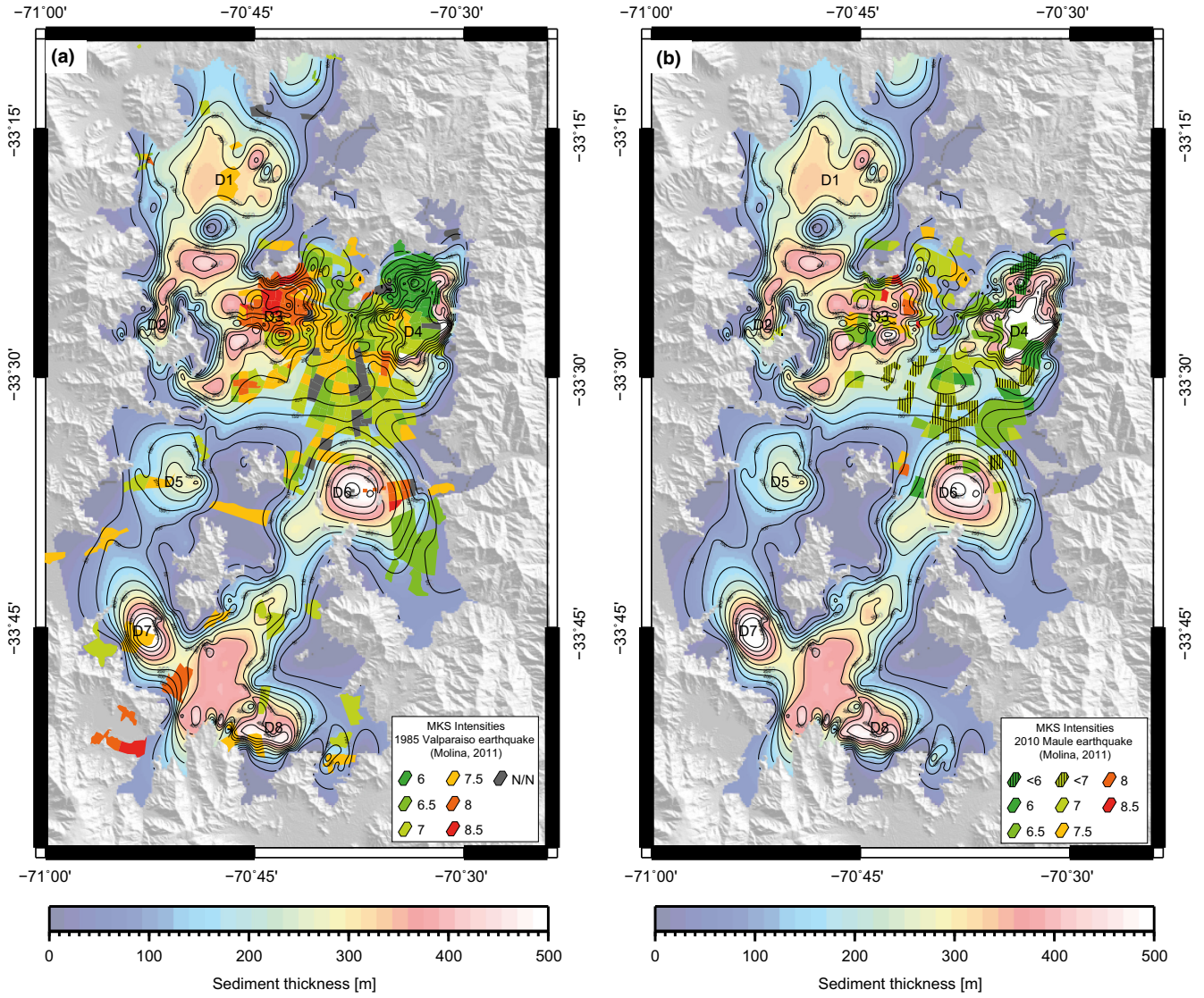

FIGURE 9 MKS seismic intensities for the 1985 Valparaiso (a) and 2010 Maule (b) earthquakes (Molina, 2011). The intensities are presented over the resultant sediment thickness model (Figure 3b) of the Santiago basin

probably related to units of diverse ages, and fault zones associated to former tectonic settings in this area.

While analysing gravity data, it was clear that no confident model of the sedimentary infill could be presented if the basement estimation is not considering the heterogeneities that are characterizing this unit. The solution presented here is a good estimation of the basement morphology, considering the available data, and according to the reliable constraints, a lower boundary for the basement depth.

The complexity of the Santiago Basin showed that the geophysical characterization of a basin should be treated with care. The presence of the strong positive anomaly in the centre of the basin and the lack of basement depth constrains were some of the difficulties encountered in the data modelling process. In future works it is essential to constrain the bedrock depth by other geophysical techniques (e.g. seismic studies) to get better results from the gravimetric modelling.

The obtained models of basement elevation highlight the importance of the erosive processes during the formation of the basin, and also provide evidence of the structural control during the process. This structural signature is observed as a slightly eastward deepening of the basement relief observed in the north-central area, portions of the basement relief located below the sea level, the presence of fault zones at the centre and to the East of the basin, and the high-density lineaments observed in the basement.

Based on the intensities of the 1985 Valparaiso and 2010 Maule earthquakes observed in Santiago, a little correlation between the more damaged areas and the location of important depocenters has been observed in the northern and central-south part of the basin, but the results are not extensive to all the depocenters and then more data are

required to better understand the role of the superficial and deep structure of the basin on the seismic amplification within the Santiago Basin. Moreover, a more complete analysis regarding a more comprehensive study of the basement geometry and depocenters could give a new perspective to the estimation of seismic risk in the most densely populated basin of Chile.

ACKNOWLEDGEMENTS

This work was funded by the Programa de Riesgo Sísmico of the University of Chile (PRS) and developed by the Núcleo de Geofísica Aplicada (NGA), Departamento de Geofísica of the University of Chile. We thank the IRD-GET for providing the CG-3 Scintrex gravimeter, and the Anillo Project (ACT N°18) and Centro de Excelencia en Geotermia de Los Andes (CEGA) FONDAP project 15090013 for providing geophysical data measured in former campaigns. A. Maksymowicz was supported by project FONDECYT 3150160 of the Chilean National Science Foundation (CONICYT). F. González acknowledges partial support from a CONICYT doctoral scholarship (21170059). None of the authors have a conflict of interest to disclose. The authors sincerely appreciate the valuable comments of the reviewers F. Horowitz and A. Folguera.

REFERENCES

Angermann, D., Klotz, J., & Reigber, C. (1999). Space-geodetic estimation of the Nazca – South America Euler vector. *Earth and Planetary Science Letters*, *171*, 329–334. https://doi.org/10.1016/S0012-821X(99)00173-9

Araneda, M., Avendaño, M., & Merlo, C. (2000). Modelo gravimétrico de la Cuenca de Santiago, etapa III final. In: Congreso Geológico Chileno, No. 9, Actas 2: 404–408.

Armijo, R., Rauld, R., Thiele, R., Vargas, G., Campos, J., Lacassin, R., & Kausel, E. (2010). The West Andean Thrust, the San Ramon Fault, and the seismic hazard for Santiago, Chile. *Tectonics*, *29*(2).

Astroza, M., Ruiz, S., Astroza, R., & Molina, J. (2012). Intensidades sísmicas. In Departamento Ingeniería Civil, Universidad de Chile (Eds.), *Mw=8.8 Terremoto en Chile, 27 de Febrero 2010* (pp. 107–126). Santiago, Chile: Departamento Ingeniería Civil, Universidad de Chile.

Bonnefoy-Claudet, S., Baize, S., Bonilla, L. F., Berge-Thierry, C., Pasten, C., Campos, J., … Verdugo, R. (2009). Site effect evaluation in the basin of Santiago de Chile using ambient noise measurements. *Geophysical Journal International*, *176*, 925–937. https://doi.org/10.1111/j.1365-246X.2008.04020.x

Charrier, R., Baeza, O., Elgueta, S., Flynn, J. J., Gans, P., Kay, S. M., … Zurita, E. (2002). Evidence for Cenozoic extensional basin development and tectonic inversion south of the flat-slab segment, southern Central Andes, Chile (33°-36°S.L.). *Journal of South American Earth Sciences*, *15*(1), 117–139. https://doi.org/10.1016/S0895-9811(02)00009-3

Díaz, D., Maksymowicz, A., Vargas, G., Vera, E., Contreras-Reyes, E., & Rebolledo, S. (2014). Exploring the shallow structure of the San Ramón thrust fault in Santiago, Chile (~ 33.5°S), using active seismic and electric methods. *Solid Earth*, *5*(2), 837. https://doi.org/10.5194/se-5-837-2014

Dragicevic, M. (1982). Nota sobre medidas de gravedad en el sector oeste de la cuenca de Santiago. *Rev. Tralka*, *2*, 207–221.

Drake, R., Curtiss, G., & Vergara, M. (1976). Potassium argon dating of igneous activity in the central Chilean andes-latitude 33°S. *Journal of Volcanology and Geothermal Research*, *1*(3), 285–295. https://doi.org/10.1016/0377-0273(76)90012-3

Echaurren, A., Folguera, A., Gianni, G., Orts, D., Tassara, A., Encinas, A., & Giménez, M. (2016). Tectonic evolution of the North Patagonian Andes (41–44°S) through recognition of syntectonic strata. *Tectonophysics*, *677–678*, 99–114. https://doi.org/10.1016/j.tecto.2016.04.009

Falcón, E., Castillo, O., & Valenzuela, M. (1970). Hidrogeología de la cuenca de Santiago. Contribución de Chile al Decenio Hidrológico Internacional. *Instituto de Investigaciones Geológicas* 51 p.

Farías, M., Charrier, R., Carretier, S., Martinod, J., Fock, A., Campbell, A., … Comte, D. (2008). Late Miocene high and rapid surface uplift and its erosional response in the Andes of central Chile (33○–35○ S). *Tectonics*, *27*, TC1005. https://doi.org/10.1029/2006tc002046

Farías, M., Comte, D., Charrier, R., Martinod, J., David, C., Tassara, A., … Fock, A. (2010). Crustal-scale structural architecture in central Chile based on seismicity and surface geology: Implications for Andean mountain building. *Tectonics*, *29*(3).

Fock, A. (2005). *Cronología y tectónica de la exhumación en el Neógeno de los Andes de Chile central entre los 33° y los 34°S*. PhD thesis, Universidad de Chile, Santiago, Chile.

Fuentes, F. (2004). *Petrología y metamorfismo de muy bajo grado de unidades volcánicas oligoceno-miocenas en la ladera occidental de los Andes de Chile Central (33° S)*. PhD thesis, Universidad de Chile, Santiago, Chile.

Gana, P., & Wall, R. (1997). Evidencias geocronológicas 40Ar/39Ar y K-Ar de un hiatus cretácico superior-eoceno en Chile central (33-33°30'S). *Andean Geology*, *24*(2), 145–163.

Giambiagi, L., Tassara, A., Mescua, J., Tunik, M., Alvarez, P., Godoy, E., … Pagano, S. (2014) Evolution of shallow and deep structures along the Maipo-Tunuyan transect (33̊40′ S): from the Pacific coast to the Andean foreland. In S. Sepúlveda, L. Giambiagi, J. Moreiras, L. Pinto, M. Tunik, G. Hoke & M. Farías (Eds.), *Geodynamic processes in the Andes of Central Chile and Argentina* (pp. 63–82). London: Geological Society.

Karzulovic, J. (1957) Sedimentos cuaternarios y aguas subterráneas en la Cuenca de Santiago. Anales de la Facultad de Ciencias Físicas y Matemáticas, Universidad de Chile, 14–55, 5–120.

Kausel, E. (1959) *Levantamiento gravimétrico de la Cuenca de Santiago*. Professional degree dissertation, Universidad de Chile, Santiago, Chile.

Leyton, F., Sepúlveda, S. A., Astroza, M., Rebolledo, S., Acevedo, P., Ruiz, S., … Foncea, C. (2011). Seismic zonation of the Santiago basin, Chile. 5th International Conference on Earthquake Geotechnical Engineering, Santiago, paper 5.6.

Li, Y., & Oldenburg, D. W. (1998). 3-D inversion of gravity data. *Geophysics*, *63*(1), 109–119. https://doi.org/10.1190/1.1444302

Longman, I. M. (1959) Formulas for computing the tidal acceleration due to the moon and the sun. *Journal of Geophysical Research*, *64*, 2351–2355.

Maksymowicz, A. (2007). *Modelo 3D del Moho bajo la zona de Chile central y oeste de Argentina (31°-34°S), utilizando funciones de recepción*. Msc. Thesis, Universidad de Chile, Santiago, Chile.

Marot, M., Monfret, T., Gerbault, M., Nolet, G., Ranalli, G., & Pardo, M. (2014). Flat versus normal subduction zones: a comparison based on 3-D regional traveltime tomography and petrological modelling of central Chile and western Argentina (29°–35°S). *Geophysical Journal International*, *199*, 1633–1654. https://doi.org/10.1093/gji/ggu355

Menéndez, P. (1991). *Atenuación de las intensidades del sismo del 3 de marzo de 1985 en función de la distancia a la zona de ruptura y del tipo de suelo*. Civil Engineering thesis, Universidad de Chile, Santiago, Chile.

Molina, J. (2011). *Intensidades sísmicas del terremoto del 27 de febrero de 2010 en las 34 comunas del Gran Santiago*. Civil Engineering thesis, Universidad de Chile, Santiago, Chile.

Nyström, J. O., Vergara, M., Morata, D., & Levi, B. (2003). Tertiary volcanism during extension in the Andean foothills of central Chile (33°15'-33°45'S). *Geological Society of America Bulletin*, *115*(12), 1523–1537. https://doi.org/10.1130/B25099.1

Pardo-Casas, F., & Molnar, P. (1987). Relative motion of the Nazca (Farallon) and South American Plate since Late Cretaceous time. *Tectonics*, *6*(3), 233–248. https://doi.org/10.1029/TC006i003p00233

Pastén, C., Sáez, M., Ruiz, S., Leyton, F., Salomón, J., & Poli, P. (2016). Deep characterization of the Santiago basin using HVSR and cross-correlation of ambient seismic noise. *Engineering Geology*, *201*, 57–66. https://doi.org/10.1016/j.enggeo.2015.12.021

Pilz, M., Parolai, S., Picozzi, M., Wang, R., Leyton, F., Campos, J., & Zschau, J. (2010). Shear wave velocity model of the Santiago de Chile basin derived from ambient noise measurements: a comparison of proxies for seismic site conditions and amplification. *Geophysical Journal International*, *182*(1), 355–367.

Porter, R., Gilbert, H., Zandt, G., Beck, S., Warren, L., Calkins, J., … Anderson, M. (2012). Shear wave velocities in the Pampean flat-slab region from Rayleigh wave tomography: Implications for slab and upper mantle hydration. *Journal of Geophysical Research*, *117*(B11301).

Ramos, V. A., Zapata, T., Cristallini, E., & Introcaso, A. (2004). The Andean thrust system – Latitudinal variations in structural styles and orogenic shortening. In K. R. McClay (Ed.), *Thrust tectonics and hydrocarbon systems: AAPG Memoir 82* (pp. 30–50). Tulsa, OK: AAPG.

Sellés, D. (1999). *La Formación Abanico en el Cuadrángulo Santiago (33°15'-33°30'S; 70°30'-70°45'O) Chile central: Estratigrafía y geoquímica*. MSc. Thesis, Universidad de Chile, Santiago, Chile.

Sellés, D., & Gana, P. (2001). Geología del área Talagante-San Francisco de Mostazal, Regiones Metropolitana de Santiago y del Libertador General Bernardo O'Higgins, Servicio Nacional de Geología y Minería, Serie Geología Básica 74: 30 p., escala 1:100.000. Santiago.

Seno, T. (2009). Determination of the pore fluid pressure ratio at seismogenic megathrusts in subduction zones: Implications for strength of asperities and Andean-type mountain building. *Journal of Geophysical Research*, *114*, B05405. https://doi.org/10.1029/2008JB005889

Tassara, A. (2005). Interaction between the Nazca and South American plates and formation of the Altiplano-Puna plateau: review of a flexural analysis along the Andean margin (15°–34°S). *Tectonophysics*, *399*, 39–57. https://doi.org/10.1016/j.tecto.2004.12.014

Thiele, R. (1980). Carta Geológica de Chile, n° 39, Hoja Santiago, Región Metropolitana, Santiago. *Instituto de Investigaciones Geológicas*, 51 p.

Thiele, R., Bobenrieth, L., & Boric, R. (1980). Geología de los cerros Renca, Ruiz y Colorado (Santiago): Contribución a la estratigrafía de Chile central. *Revista Comunicaciones*, *30*, 1–14.

Vergara, M., López-Escobar, L., Palma, I., Hickey-Vargas, R., & Roeschmann, C. (2004). Late Tertiary episodes in the area of the city of Santiago de Chile: new geochronological and geochemical data. *Journal of South American Earth Sciences*, *17*, 227–238. https://doi.org/10.1016/j.jsames.2004.06.003

Vergara, M., Morata, D., Villarroel, R., Nyström, J., & Aguirre, L. (1999). 40Ar/39Ar Ages, very low-grade metamorphism and geochemistry of the volcanic rock from 'Cerro El Abanico', Santiago Andean Cordillera (33°30'S, 70°30'-70°25'W). In: International Symposium on Andean Geodynamics (ISAG), 4, 785–788.

Yáñez, G., Muñoz, M., Flores-Aqueveque, V., & Bosch, A. (2015). Gravity derived depth to basement in Santiago Basin, Chile: implications for its geological evolution, hydrogeology, low enthalpy geothermal, soil characterization and geo-hazards. *Andean Geology*, *42*(2), 147–172.

SUPPORTING INFORMATION

Additional Supporting Information may be found online in the supporting information tab for this article.

How to cite this article: González FA, Maksymowicz A, Díaz D, et al. Characterization of the depocenters and the basement structure, below the central Chile Andean Forearc: A 3D geophysical modelling in Santiago Basin area. *Basin Res*. 2018;30:799–815. https://doi.org/10.1111/bre.12281